

# Structural, Optical and dielectric properties of Sr doped LaVO<sub>4</sub>

Khalid Sultan<sup>1,\*</sup>, Rubiya Samad<sup>1</sup>, Feroz A. Najjar<sup>1</sup>, Shohaib Abass<sup>1</sup>, Saima Jahan<sup>1</sup>, Mudasir Rashid Rather<sup>1</sup>, M. Ikram<sup>2</sup>

<sup>1</sup>Department of Physics, Central University of Kashmir, Tullamullah Ganderbal, J&K 191131, India

<sup>2</sup>Department of Physics, National Institute of Technology Hazratbal Srinagar, J&K 190006, India

\*Corresponding author; E-mail: ksbhat.phy@gmail.com; Tel.: (+91) 9419031528

DOI: 10.5185/amlett.2021.061640

Polycrystalline bulk samples of chemical composition La<sub>1-x</sub>Sr<sub>x</sub>VO<sub>4</sub> (x = 0.0, 0.1, 0.3, 0.5) were prepared by solid state reaction method. The Morphology and structure was characterised by Scanning Electronic microscopy and powder X-ray diffraction respectively. All the prepared material were single-phase and co-doped ions were successfully incorporated in LaVO<sub>4</sub> lattice. The EDAX spectrum shows that the percentage composition of given elements in the proposed formula was in good agreement with the corresponding values determined experimentally. The Raman spectra of LaVO<sub>4</sub> reflect the VO<sub>4</sub> type structure that consists of four different V–O bands. The prominent Raman band at about 860 cm<sup>-1</sup> can be assigned to the symmetric V–O stretching mode while the weak Raman band at 792 cm<sup>-1</sup> is assigned to antisymmetric V–O stretching mode. With increase in Sr doping, optical band gap was found to decrease resulting in increase in conductivity. The dielectric constant as well as dielectric loss shows a relaxor type of behaviour for higher doping concentration which can be attributed to the chemical pressure induced in LaVO<sub>4</sub> with the doping of Sr ions. The studies performed on ac conductivity identifies that the conduction mechanism follows the charge hopping between localised states and follow the small polaron conduction.

## Introduction

Orthovanadates have technological importance with applications as scintillators, thermophosphors, or photocatalysis materials, ionic conductors, non-linear optical material, lithium-ion batteries, and in cathodoluminescence [1-3]. Orthovanadates have attracted considerable research interest as photocatalysts due to potential applications in renewable energy and alternative green technology [4]. Orthovanadates when doped with trivalent impurities have application as laser-host materials due to their high-optical conversion efficiency, high birefringence, and good thermal conductivity [5-7]. In addition, orthovanadate nanoparticles because of their luminescent properties, chemical stability, and nontoxicity, can be used in biomedical applications [8-10].

The LaVO<sub>4</sub> orthovanadates, which are the focal point of this report, can likewise be utilized as thermophosphors, ionic conductors, and non-linear optical materials [11-14]. What's more, their doping with trivalent rare earth cations makes them very valuable as laser-host materials [15]. Indeed, YVO<sub>4</sub>, which can be developed as a single crystal utilizing various methods and is one of the most generally utilized materials in the laser business. What's more, mixes like LuVO<sub>4</sub> and YbVO<sub>4</sub> have been seen as promising materials for self-Raman lasers. On the other hand, rare earth mixes are generally utilized in numerous practical applications due to their impossible to

miss properties beginning from special electronic structure and various transition modes including 3d and 4f shell of lanthanide [16-27].

Finally, the combination of the two that is rare-earth vanadates show interesting structural and magnetic transformations at low temperatures [28] and a few are incomparable undergoing Jahn–Teller distortion [29]. Lanthanide (Ln<sup>3+</sup>) orthovanadate possessing chemical formula ABO<sub>4</sub> (where A is lanthanide and B = vanadate) are technologically important materials with immense applications as catalysis, efficient phosphors, low threshold laser host, solid-state protonic conductor and polarizer [30-31]. Lanthanum orthovanadate LaVO<sub>4</sub> has attracted much interest of the researchers for the last one decade both from a fundamental point of view and from the prospect of applications due to its surface catalytic properties. Being the binary oxide of vanadium, it is effectively utilized as catalysts for vapor phase dehydrogenation of paraffin's [32]. La<sub>x</sub>Sr<sub>1-x</sub>VO<sub>4</sub> doped lanthanum vanadates have been broadly studied for their basic, magnetic and conductive properties [33,34], while vanadates containing V<sup>5+</sup> are being studied for the specific oxidative dehydrogenation of propane, butane and ethylbenzene [35,36]. Reduced and oxidized lanthanum vanadates doped with strontium have been studied by Trikalitis *et. al.*, for their surface catalytic properties. Lanthanum orthovanadate is also considered as a promising host for luminescent lanthanide ions [37,38].

Lanthanum orthovanadate has been prepared and characterized by many authors [39-42]. However, in the literature, there has been no report of frequency and temperature dependence of dielectric properties. In the present study,  $\text{LaSrVO}_4$  has been prepared and then their structural, optical, and dielectric properties have been studied. Intended in this work is to increase the dielectric constant with the replacement of Sr for La particles and to decrease the optical band gap with Sr doping and to bring about increment in conductivity in the compound.

### Experimental procedure

Polycrystalline bulk samples of substance creation  $\text{La}_x\text{Sr}_{1-x}\text{VO}_4$  ( $x = 0.0, 0.1, 0.3, 0.5$ ) were synthesized by solid state reaction technique. The high purity (> 99.9%) antecedents of  $\text{La}_2\text{O}_3$ ,  $\text{Sr}_2\text{O}_3$  and  $\text{V}_2\text{O}_3$  taken in the stoichiometry proportion were blended and preheated at  $1000^\circ\text{C}$  for 12 hours and afterward calcinated again at  $1200^\circ\text{C}$  for 12 hours. The homogenous powder was reground into pellets and afterward was sintered at  $1300^\circ\text{C}$  for 24 hours at a warming pace of  $4^\circ\text{C min}^{-1}$  and afterward cooled to room temperature at a cooling pace of  $3^\circ\text{C min}^{-1}$  in a tubular furnace. The calcinated material was analyzed by X-ray diffraction (XRD) utilizing Bruker D8 Advance diffractometer (Cu- $K\alpha$  radiation). The diffraction edge ( $2\theta$ ) range between  $20$ - $80^\circ$  was scanned at room temperature. Raman spectra were recorded with a Labram-HR800 miniaturized scale Raman spectrometer furnished with a Peltier cooled charge-coupled gadget indicator utilizing an Ar excitation source with wavelength of 488 nm. Neither melting nor any phase transition was observed in the sample at excitation of Laser intensity of 10 mW. The SEM micrographs and EDX examination were obtained utilizing JSM-6490LV Joel. The picture solution was set at 5,000X and 10,000X. Bulk Samples of  $\text{LaVO}_4$  were dissolved in ethanol and illuminated under ultra violet radiation to see the impact of Sr doping on maximum absorption wavelength and hence on optical properties of systems. Electrical properties were studied by an impedance analyzer by Wayne Kerr Electronics. This instrument straightforwardly gives the estimations of capacitance (C) and dielectric loss ( $\tan \delta$ ) which were utilized to ascertain other electric amounts. The information was recorded in the recurrence scope of 20 Hz – 3MHz and temperature scope of  $20$ - $380^\circ\text{C}$  in air. The temperature was controlled at a pace of  $2^\circ\text{C min}^{-1}$  by a chip-based furnace.

### Results and discussions

#### XRD analysis of $\text{La}_{1-x}\text{Sr}_x\text{VO}_4$ ( $x = 0.0, 0.1, 0.3, 0.5$ )

The X-ray diffraction patterns of  $\text{La}_{1-x}\text{Sr}_x\text{VO}_4$  ( $x = 0.0, 0.1, 0.3, 0.5$ ) Samples are shown in Fig. 1. The XRD data of all the samples were analyzed using Powder-X software which clearly indicates the single-phase formation with space group  $P_2$ . The calculated XRD parameters of all the samples are shown in Table 1. With increase in Sr content, the lattice constants  $a$  and  $c$  decreases while the

lattice constant  $b$  increases with Sr at higher concentration. The Cell volume slightly decreases while as the interplanar distance changes slightly because the angle of peak ( $q$ ) does not vary significantly after Sr doping.

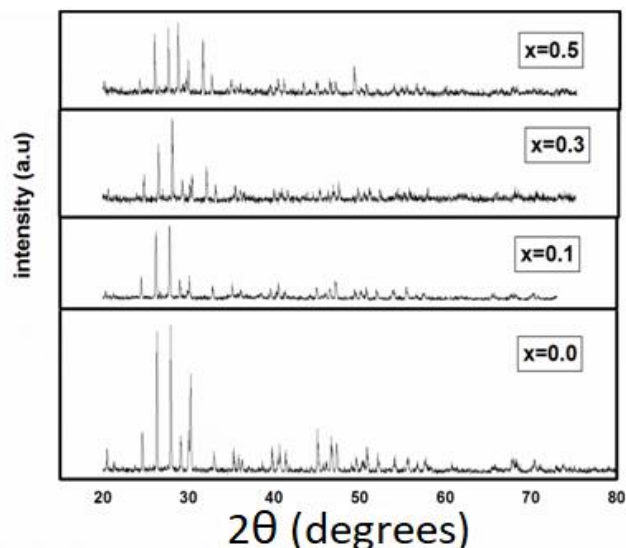


Fig. 1. X-ray diffraction patterns of  $\text{La}_{1-x}\text{Sr}_x\text{VO}_4$  ( $x = 0.0, 0.1, 0.3, 0.5$ ).

Table 1. XRD parameters of  $\text{La}_{1-x}\text{Sr}_x\text{VO}_4$  ( $x=0.0, 0.1, 0.3, 0.5$ )

Sample	X=0.0	X=0.1	X=0.3	X=0.5
$\text{La}_{1-x}\text{Sr}_x\text{VO}_4$				
Space group	$P 2_1/n$	$P 2_1/n$	$P 2_1/n$	$P 2_1/n$
$a(\text{Å})$	7.05057	7.07849	7.07252	7.06894
$b(\text{Å})$	7.2868	7.20903	7.20182	7.29221
$c(\text{Å})$	6.73102	6.67837	6.66952	6.7353
$\beta$	104.9143	104.07558	104.0696	104.88053
Volume	331.097	330.559	329.521	335.549

#### Morphological studies and elemental analysis of $\text{La}_{1-x}\text{Sr}_x\text{VO}_4$ ( $x = 0.0, 0.1, 0.3, 0.5$ )

The detailed morphological investigations of the samples were made utilizing the scanning electron microscope. SEM micrographs of  $\text{La}_{1-x}\text{Sr}_x\text{VO}_4$  ( $x = 0.0, 0.1, 0.3, 0.5$ ) sintered at  $1300^\circ\text{C}$  for 24 h are shown in Fig. 2. The microstructure uncovers that the particles are circular fit as a fiddle with mean particle size of  $5\mu\text{m}$ . It is obvious from Fig. 2 that the normal grain size increases with the increase in Sr doping which may bring about increment in dielectric constant. So as to distinguish the presence and the atomic percentage of La, V, Sr and oxygen, the energy dispersive analysis of X-rays (EDAX) was performed utilizing a energy dispersive spectrometer (OXFORD ISIS-300 framework) appended to a SEM JEOL JSM-6490LV. Fig. 2 shows the EDAX range of  $\text{La}_{1-x}\text{Sr}_x\text{VO}_4$  ( $x = 0.0, 0.1, 0.3, 0.5$ ). The presence of La, Sr and V is unmistakably found in the range. The weight level of La, Sr and V as got by EDAX is appeared in Table 2. The percentage composition of given components in the proposed recipe concurs well with the corresponding determined experimentally as appeared in Table 2.

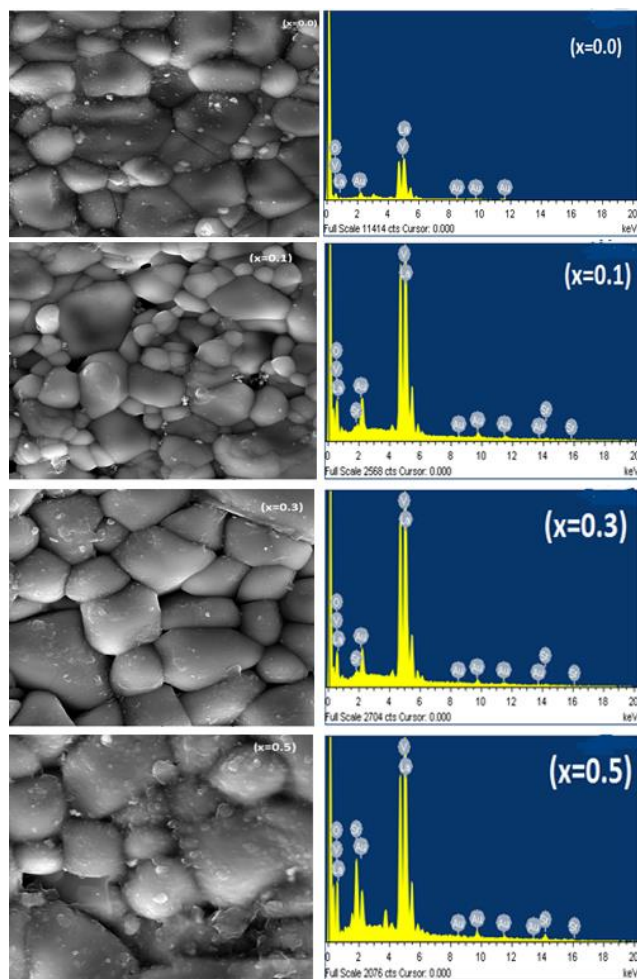


Fig. 2. SEM micrograph and EDAX spectrum of  $\text{La}_{1-x}\text{Sr}_x\text{VO}_4$  ( $x = 0.0, 0.1, 0.3, 0.5$ )

Table 2. The calculated and experimental weight percentage of La, V, O, Sr.

Compound	Element	Experimental (Weight %)	Theoretical (Weight %)
LaVO <sub>4</sub>	O	24.87	25.205
	V	19.12	20.0701
	La	56.01	54.7241
La <sub>0.9</sub> Sr <sub>0.1</sub> VO <sub>4</sub>	O	26.20	25.7225
	V	19.88	20.4816
	La	51.08	50.2616
	Sr	2.84	3.5341
La <sub>0.7</sub> Sr <sub>0.3</sub> VO <sub>4</sub>	O	26.28	26.8225
	V	19.63	21.3574
	La	43.96	40.76407
	Sr	10.13	11.05593
La <sub>0.5</sub> Sr <sub>0.5</sub> VO <sub>4</sub>	O	30.84	28.0207
	V	21.63	22.3115
	La	29.37	30.4179
	Sr	18.16	19.2497

### Raman study of $\text{La}_{1-x}\text{Sr}_x\text{VO}_4$ ( $x = 0.0, 0.1, 0.3, 0.5$ )

Raman investigation of the synthesized samples were completed and the spectra were collected in back scattering geometry utilizing an Ar excitation source having a wavelength of 488 nm combined with a Labram-

HR800 micro scale Raman spectrometer outfitted with a 50X target, proper step channel and a Peltier cooled charge-coupled gadget identifier. No phase transition or melting was seen in the samples at excitation Laser intensity of 10 mW. Fig. 3 shows the Raman spectra of the samples at room temperature. The positions allotted to extraordinary Raman peaks are  $860\text{ cm}^{-1}$  and  $370\text{ cm}^{-1}$ . Other than this more fragile groups are noticeable at 818, 792, 345, 328, 206 and  $147\text{ cm}^{-1}$ . The Raman spectra of LaVO<sub>4</sub> reflect the VO<sub>4</sub> type structure that comprises of four distinctive V–O groups. The most extreme Raman band at around  $860\text{ cm}^{-1}$  can be assigned to the symmetric V–O extending mode (Ag symmetry), while the weak Raman band at  $792\text{ cm}^{-1}$  is allocated to antisymmetric V–O stretching mode (Bg symmetry), the symmetric (Ag) and antisymmetric (Bg) bending modes are at 370 and around  $345\text{ cm}^{-1}$  respectively, and outer modes (rotation/translation) happen at 206 and  $147\text{ cm}^{-1}$  [43]. The Raman groups and their assignments have been accounted for in Table 3. The situation for the allotted Raman groups appeared in this examination has a likeness to the bismuth vanadate tests with comparable monoclinic structure additionally containing VO<sub>4</sub> tetrahedron [44]. From the figure it very well may be seen that Sr doping doesn't move the Raman groups to higher frequencies.

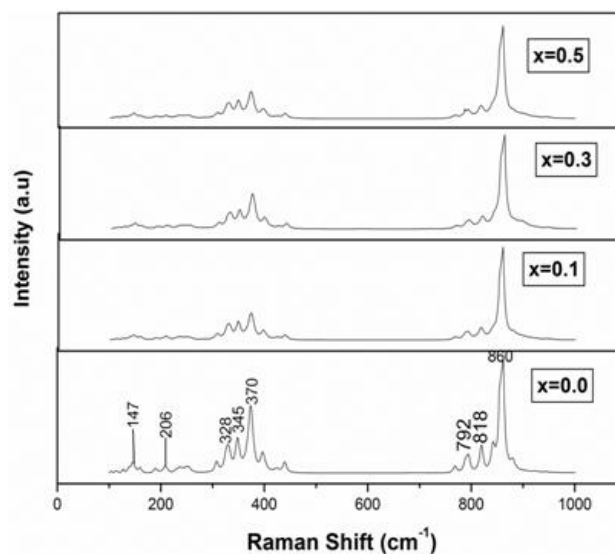


Fig. 3. Raman spectra of  $\text{La}_{1-x}\text{Sr}_x\text{VO}_4$  ( $x = 0.0, 0.1, 0.3, 0.5$ ).

Table 3. The observed Raman modes with corresponding atomic motion for  $\text{La}_{1-x}\text{Sr}_x\text{VO}_4$  ( $x = 0.0, 0.1, 0.3, 0.5$ ).

Position	Assignments	Symmetry
147	La-O Rot/trans	External
206	La-O Rot/trans	External
345	Antisymmetric V-O bending mode	Bg symmetry
370	Symmetric V-O bending mode	Ag symmetry
792	Antisymmetric V-O stretching mode	Bg symmetry
860	Symmetric V-O stretching mode	Ag symmetry

**Optical study of  $La_{1-x}Sr_xVO_4$  ( $x = 0.0, 0.1, 0.3, 0.5$ )**

The optical band gap  $E_g$  was determined from the curve between  $(\alpha \cdot hv)^{1/2}$  and  $E$  (eV) where  $\alpha$  is the absorption coefficient and  $E$  is energy in electron volts (Fig. 4). The compositional estimations of  $E_g$  are appeared in Table 3. Also, obviously the optical band gap diminishes with increment in Sr doping bringing about increment in conductivity with Sr doping. The optical outcomes are predictable with other dielectric results (as discussed in next section).

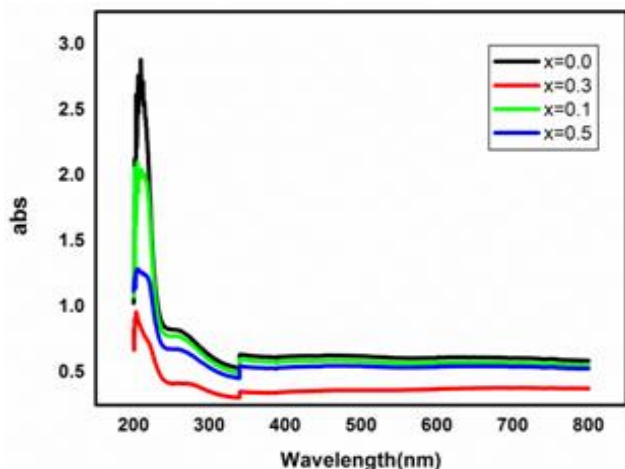


Fig. 4. UV-Vis spectra of  $La_{1-x}Sr_xVO_4$  ( $x = 0.0, 0.1, 0.3, 0.5$ ).

**Dielectric properties of  $La_{1-x}Sr_xVO_4$  ( $x = 0.0, 0.1, 0.3, 0.5$ )**

The dielectric estimations were done in a frequency range 20 Hz – 3 MHz and temperature range 20 – 250°C utilizing a Wayne Kerr Impedance Analyzer Model 1J43100 and further automated by utilizing a PC for information recording, storage and information. A chip-based furnace fitted with a temperature controller and an extraordinarily structured two-terminal sample holder was utilized to warm the sample at a warming pace of 2°C min<sup>-1</sup>. The high impedance analyzerutilized in the current examination legitimately gives the estimations of capacitance  $C$  and dielectric loss. Different boundaries, for example, dielectric consistent  $\epsilon'$  and ac conductivity,  $\sigma$  are processed utilizing the relations:

$$\epsilon' = \frac{C t}{\epsilon_0 A} \quad \text{and} \quad \sigma = 2\pi f \epsilon_0 \epsilon' \tan \delta$$

where,  $C$  is capacitance (in Farad),  $t$  is thickness (in meters),  $A$  is area (in m<sup>2</sup>),  $\epsilon_0 = 8.854 \times 10^{-12} \text{ Fm}^{-1}$ ,  $f$  is the frequency (in Hz) of the applied electric field and  $\sigma$  the ac conductivity (in  $\Omega^{-1}\text{m}^{-1}$ ).

It is seen from Fig. 5 that dielectric constant decreases with the increase in frequency for all the compositions of  $La_{1-x}Sr_xVO_4$  ( $x = 0.0, 0.1, 0.3, 0.5$ ). The decline of dielectric constant with increment of frequency is an ordinary dielectric conduct and can be clarified based on polarization system. There are four essential instruments of polarization in materials i.e., electronic, ionic or

nuclear, dipolar or orientational and space charge or interfacial polarization. At low frequencies, all the components of polarization add to the dielectric constant. With the increase in frequency, the commitments from various polarizations begin diminishing. The high rise of dielectric constant at lower frequencies might be credited to space charge polarization because of grain limit impacts. From the figure, it is unmistakably observed that dielectric constant increases with increase in Sr doping. The variation of dielectric loss with frequency for all the synthesized samples are given in Fig. 6. The nonattendance of any loss peak in the dielectric dispersion of the material (Fig. 6) recommends its conduct to be that of low frequency dispersion (LFD) or the semi dc process (QDC) [44-47]. It ought to be noticed that dipolar framework will show loss peaks, while carrier dominated systems display QDC reactions.

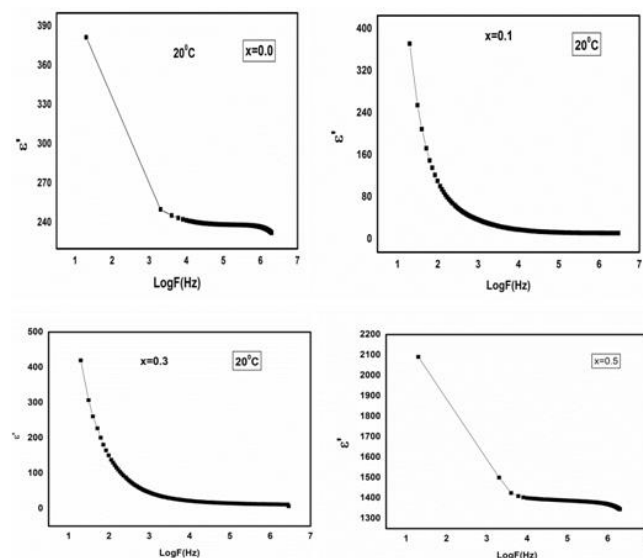


Fig. 5. Variation of dielectric constant with frequency of  $La_{1-x}Sr_xVO_4$  ( $x = 0.0, 0.1, 0.3, 0.5$ ) at 20 °C.

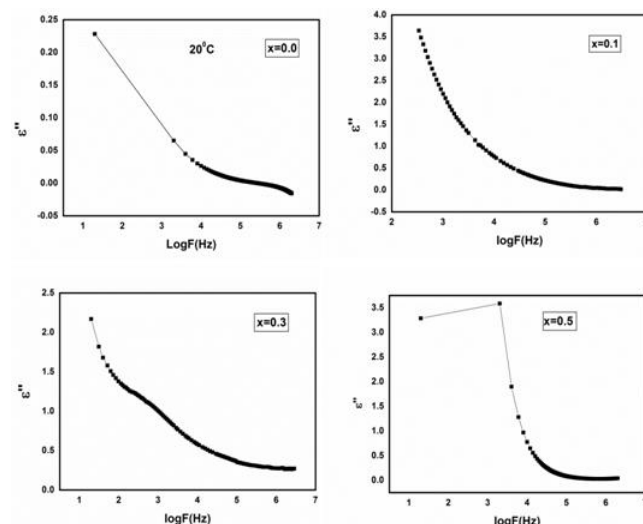


Fig. 6. Variation of dielectric loss versus frequency of  $La_{1-x}Sr_xVO_4$  ( $x = 0.0, 0.1, 0.3, 0.5$ ).

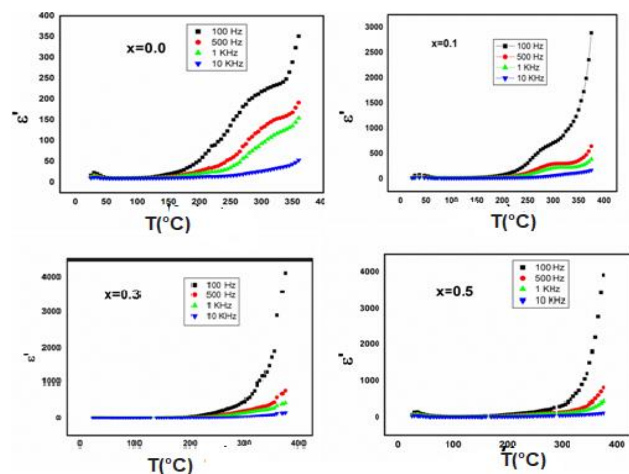


Fig. 7. Variation of dielectric constant with temperature of La<sub>1-x</sub>Sr<sub>x</sub>VO<sub>4</sub> (x = 0.0, 0.1, 0.3, 0.5).

### Temperature dependence of dielectric properties

The temperature reliance of dielectric constant ( $\epsilon'$ ) and dielectric loss tangent ( $\tan \delta$ ) at various frequencies for La<sub>1-x</sub>Sr<sub>x</sub>VO<sub>4</sub> (x = 0.0, 0.1, 0.3, 0.5) are presented in Fig. 7 and Fig. 8 separately. From Fig. 7, clearly the dielectric constant doesn't shift at low temperature while at higher temperature it increases for all the samples. Such a conduct at higher temperature is because of generation of additional thermal energy which upgrades the portability of charge transporters henceforth builds rate of hopping. At low temperatures, the thermal energy isn't adequate to add to the portability of charge transporters. This observed mechanism sets up the higher polarization at higher temperature which expands the dielectric constant. For higher doping concentrations, both dielectric loss and dielectric constant shows a relaxor kind of conduct which can again be ascribed to the chemical pressure actuated in LaSrVO<sub>4</sub> with the doping of Sr particles. The changes in the oxidation state of La ions brought about by the divalent Sr ions to maintain charge stability in the compound induces more dielectric loss into the system.

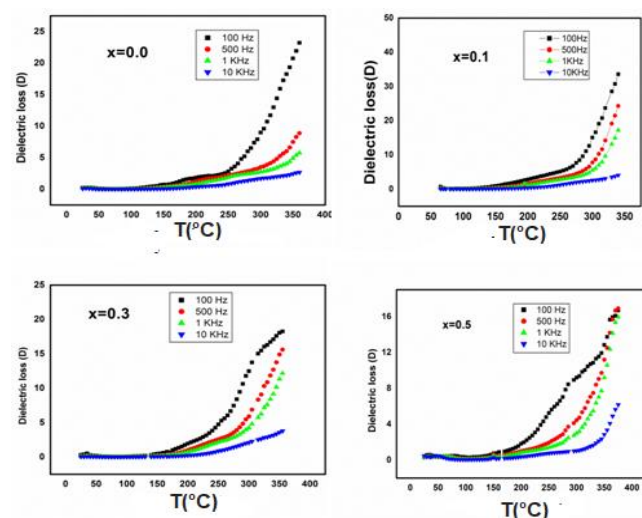


Fig. 8. Variation of dielectric loss with temperature of La<sub>1-x</sub>Sr<sub>x</sub>VO<sub>4</sub> (x = 0.0, 0.1, 0.3, 0.5).

### AC conductivity of La<sub>1-x</sub>Sr<sub>x</sub>VO<sub>4</sub> (x = 0.0, 0.1, 0.3, 0.5)

To comprehend the system of conduction and the kind of polarons answerable for conduction, ac conductivity ( $\sigma_{ac}$ ) was determined utilizing the accompanying connection:

$$\sigma_{ac} = 2\pi f \epsilon_0 \epsilon' \tan \delta$$

where,  $\epsilon_0 = 8.854 \times 10^{-12}$  F m<sup>-1</sup> and f is the recurrence (in Hz) of the applied electric field. Fig. 9 shows the temperature dependent (at chosen frequencies) ac conductivity plots separately. A straight conduct is watched for ac conductivity with temperature for all frequencies at low temperature, and shows a sharp increment at higher frequencies, which might be credited to the expansion in the quantity of charge carriers and their floated portability which are thermally activated. With the increase in doping, ac conductivity increases. The ac conductivity increases with frequency and the outcomes obtained are in acceptable concurrence with the literature [48-49]. The ac conductivity modification recognizes that the conduction system is following the charge hopping between localized states. The observed outcomes follow small polaron conduction and are reliable with the literature [50-52]. The hopping frequency of charge transporters is by all accounts the capacity of the frequency of the applied field which brings about increment in mobility of charge carriers. Since the conductivity isn't enhanced by charge transporters rather it increases as a result of mobility of these carriers, in this manner at certain higher frequencies, the hopping of charge carriers stops to follow the applied field frequencies and decrease in conductivity. The comparison shows a marked difference in the conductivity behavior of pure and doped LSVO samples among which the pure sample shows a stronger temperature as well as the frequency dependence. As evident, the conductivity ( $\sigma_{ac}$ ) is showing an increasing trend for both the increasing temperature as well as increasing frequency, this behavior unfolds the nature of LSVO to be semiconducting.

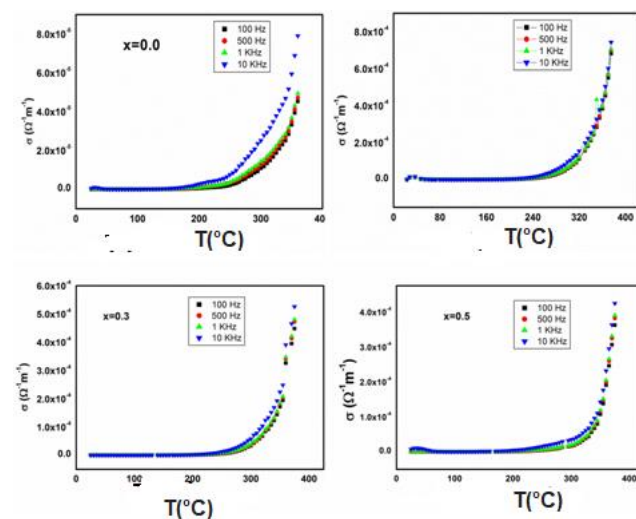


Fig. 9. Variation of ac conductivity with temperature of La<sub>1-x</sub>Sr<sub>x</sub>VO<sub>4</sub> (x = 0.0, 0.1, 0.3, 0.5).

## Conclusion

Polycrystalline bulk samples of Sr doped LaVO<sub>4</sub> were synthesized by solid state reaction procedure. The replacement of Sr for La particles results in huge changes in the physical properties of compound. The incorporation of Sr clearly brings a distortion the crystal structure, which is reflected in XRD and Raman study. The results of dielectric study show there is increase in dielectric constant particularly at higher doping. The higher dielectric constant and higher ac conductivity drove the material appropriate for power application as these may empower gadget scaling down (device miniaturization). Optical band gap of the compound was likewise observed to diminish with Sr doping bringing about increment in conductivity in the compound. The ac conductivity adjustment recognizes that the conduction component follows the charge hopping between localized states and follow the small polaron conduction. The current examination plainly shows that the physical properties of Sr doped LaVO<sub>4</sub> rely upon the measure of doping and thus on the charge state involved by Sr and La particles.

**Keywords:** Doping, XRD, space group, dielectric study, ac conductivity.

**Received: 2 December 2020**

**Revised: 9 December 2020**

**Accepted: 10 January 2021**

## Références

- Errandonea, D.; Garg, A. B.; *Progress in Materials Science*, **2018**, *97*, 123.
- Jia, C.J.; Sun, L.D.; Luo, F.; Jiang, X.C.; Wei, L.H.; Yan, C.H.; *Appl Phys Lett.*, **2004**, *84*, 5305.
- Kaminskii A.A.; Lux, O.; Rhee, H.; Eichler, H.J.; Ueda, K.; Oka, K.et.al.*Appl Phys B.*,**2008**, *93*,865.
- Fukudome, K.; Ikenaga, N.; Miyake, T.; Suzuki, T.; *Catal. Sci. Technol.*, **2011**, *1*, 987.
- Hou, Z.; Yang, P.; Li, C.; Wang, L.; Lian, H.; Quan, Z. et. al.; *Chem Mater*, **2008**, *20*, 6686.
- Zhang, H.; Fang, H.S.; Zheng, L.L.; Hu, Z.G.; Zhang, G.C.; *J. Cryst Growth*, **2009**, *311*, 4652.
- Kaminskii, A.A.; Lux, O.; Rhee, H.; Eichler, H.J.; Ueda, K.; Yoneda, H. et. al.; *Laser Phys Lett.*, **2012**, *9*, 879.
- Abdesselem, M.; Schoeffel, M.; Maurin, I.; Ramodiharilafy, R.; Autret, G.; Clement, O.et. al.; *ACS Nano*, **2014**, *8*, 11126.
- Goltsev, A.N.; Babenko, N.N.; Gaevskaya, Y.A.; Chelombitko, O.V.; Dubrava, T.G.; Bondarovich, N.A.; *Biotechn Acta*, **2015**, *8*, 113.
- Li, D.; Liu, C.; Jiang, L.; *Opt Mater.*, **2015**, *48*, 18.
- Ishihara, S.; *Phys. Rev. Lett.*, **2005**, *94*, 156408.
- Ishiharaand, S.; Hatakeyama, T.; *J. Mag. Mag. Mater.*, **2004**, *272*, 412.
- Ulrich, C.; Khaliullin, G.; Mirker, C.; *Phys. Rev. Lett.*, **2003**, *91*, 257202.
- Fang, Z.; Nagaosa, N.; Terakura, K.; *Phys. Rev. B.*, **2003**, *67*, 035101.
- Miyasakal, S.; Okimoto, Y.; Tolura, Y.; *J. Phys. Soc. Jpn.*, **2002**, *71*, 2086.
- Bleaney, B.; Pfeffer, J. Z.; Wells, M. R.; *J. Phys. Condens. Matter.*, **1997**, *9*, 7469.
- Motome, Y.; Seo, H.; Fang, Z.; *Phys. Rev. Lett.*, **2003**, *90*, 146602.
- Yan, J.Q.; Zhou, J.S. Goodenough, J.B.; *Phys. Rev. Lett.*, **2004**, *93*, 235901
- Duclos, S.J.; Jayaraman A.; Espinosa G.P.; Cooper, ASJ.; *J. Phys. Chem Solids*, **1989**, *50*, 769.
- Chen, G.; Stump, N.A.; Haire, R.G.; Peterson, J.R.; Abraham, M.; *Solid State Commun.*,**1992**, *84*, 313.
- Garg, A.B.; Errandonea, D.; Rodriguez-Hernandez, P.; López-Moreno, S.; Muñoz, A.; Popescu, C.; *J. Phys. Cond. Matter.*, **2014**, *26*, 265402.
- Hong, F.; Yue, B.; Cheng, Z.; Shen, H.; Yang, K.; Hong, X. et. al.; *Appl. Phys. Lett.*, **2017**, *110*, 021903.
- Yue, B.; Hong, F.; Merkel, S.; Tan, D.; Yan, J.; Chen, B. et. al.; *Phys. Rev. Lett.*, **2016**, *117*, 135701.
- Rice, C.E.; Robinson, W.R.; *Acta Cryst B.*, **1976**, *32*, 2232.
- Errandonea, D.; Pellicer-Porres, J.; Martinez-Garcia, D.; Ruiz-Fuertes, J.; Friedrich, A.; Morgenroth, W. et. al.; *J. Phys. Chem. C.*, **2016**, *120*, 13749.
- Cheng, X.; Guo, D.; Feng, S.; Yang, K.; Wang, Y.; Ren, Y. et. al.; *Opt. Mater.*, **2015**, *49*, 32.
- Ruiz-Fuertes, J.; Gomis, O.; León-Luis, S.F.; Schrodt, N.; Manjón, F.J.; Ray, S. et. al.; *Nanotechnology*, **2016**, *27*, 025701.
- Ghering, G. A.; Ghering, K. A.; *J. Mater. Sci. Lett.*, **1975**, *2*, 71.
- Smith, S. H.; Wanklyn, B.M.; *J. Cryst. Growth*, **1974**, *21*, 23.
- Guttman, A. T.; Brazdil, J. F.; Grasselli, P. K.; US Patent, **1989**, *4*, 816.
- Balasubramanian, M. R.; *J. Indian Chem. Soc.*, **1978**, *64*, 453.
- Reuter, B.; Vollnik, M.; *Naturwissenschaften*, **1963**, *50*, 569.
- Egdell,R. G.; Harrison, M. R.; Hill, M. D.; Porte, L.; Wall, G.; *J. Phys. C*, **1984**, *17*, 2899
- Dougier, P.; Casalot, A.; *J. Sol. Stat. Chem.*, **1970**, *15*, 346[17],  
Dougier, P.; Hagenmuller, P.; *J. Sol. Stat. Chem.*, **1975**, *15*, 158.
- Kung, M.C.; Kung, H. H.; *J. Catal.*, **1992**, *134*, 668.
- Gao, X.; Ruitz, P.; Xin, Q.; Delmon, B.; *J. Catal.*, **1994**, *148*, 56.
- Chang, W.S.; Chen, Y.S.; Yang, B. L.; *Appl. Catal. A: General*, **1995**, *124*, 221.
- Trikalitis, P. N.; Bakas, T. V.; Moukarika, A. C.; Sdoukos, A. T.; Angelidis, T.; Pomonis, P. J.; *Appl. Catal. A.*, **1998**, *167*,295.
- Wang, X.; Loa, I.; Syassen, K.; Hanfland, M.; Ferrand, B.; *Phys. Rev. B.*,**2004**, *70*, 064109.
- Errandonea, D.; Lacomba-Perales, R.; Ruiz-Fuertes, J.; Segura, A.; Achary, S.N.; Tyagi, A.K.; *PhysRev B.*, **2009**, *79*, 184104.
- Garg, A.B.; Errandonea, D.; Rodriguez-Hernandez, P.; López-Moreno, S.; Muñoz, A.; Popescu C.; *J. Phys. Cond. Matter.*, **2014**, *26*, 265402.
- Paszkwicz, W.; Lopez-Solano, J.; Piszora, P.; Bojanowski, B.; Mujica, A.; Munoz, A., et. al.; *J. Alloys Compd.*, **2015**, *648*, 1005.
- Hardcastle, F.D.; Wachs, I.E.; Eckert, H.; Jefferson, D.A.; *J. Sol. Stat. Chem.*, **1991**, *90*, 194.
- Gotic, M.; Music, S.; Ivandaa, M.; Soufek, M.; Popovic, S.; *J. Mol. Struc.*, **2005**, *535*,744.
- Jonscher, A.K.; *Colloid Polym Sci.*, **1975**, *253*, 231.
- Dissado, L.A.; Hill, R.M.; *Proc Roy Soc London*, **1983**, *390*, 131.
- Dissado, L.A.; Hill, R.M.; *J. Chem Soc Faraday Trans.*,**1984**, *80*, 291.
- Jonscher, A.K. The universal dielectric response and its physical significance. *IEEE Trans Electron Insul.*, **1992**, *27*, pp.407-423.
- Lokare, S.A.; Devan, R.S.; Chougule, B.K.; *J. Alloys Compd.*, **2008**, *454*,471.
- Devan, R.S.; Kolekar, Y.D.; Chougule, B.K.; *J. Alloys Compd.*, **2008**, *461*, 678.
- Patankar, K.K.; Joshi, S.S.; Chougule, B.K.; *Phys. Lett. A.*, **2005**, *346*, 337.
- Adler, Feinleib.; *J. Phys Rev B.*,**1970**, *2*, 3112.